ELSEVIER

Contents lists available at ScienceDirect

Chaos, Solitons and Fractals

journal homepage: www.elsevier.com/locate/chaos



Multifractality analysis of phase transition of the two- and three-dimensional XY models

Marcos A.A. de Sousa ^a, Francisco A.B.F. de Moura ^{a,b}, Anderson L.R. Barbosa ^a, Adauto J.F. de Souza ^a, **,

ARTICLE INFO

Keywords: XY model Multifractality Phase transition Hurst exponent Singularity spectrum

ABSTRACT

We performed an extensive investigation of the multifractal features of time series for magnetization and helicity moduli for the XY model in two and three dimensions. We employed multifractal analysis to extract generalized Hurst exponents and singularity spectra, enabling us to quantify the degree of multifractality across different temperatures. Our results show that multifractality is maximized near the critical points, with broader singularity spectra in the two-dimensional system, which is consistent with the Berezinskii-Kosterlitz-Thouless transition. In three dimensions, the multifractal signatures are sharper and more localized, reflecting the second-order nature of the transition. These findings confirm multifractality as a robust tool that captures essential features of both conventional and topological phase transitions.

1. Introduction

Complex systems are composed of many nonlinearly interacting elements that give rise to emergent phenomena, whose collective behavior cannot be simply inferred from the knowledge of the microscopic interactions alone [1]. One of their most remarkable features is the ability to self-organize, often leading to the spontaneous appearance of coherent structures and long-range correlations [2,3]. Such emergent order is not restricted to physical systems: it is also observed in biological networks, ecosystems, financial markets, and even in patterns of human activity, indicating the ubiquity of these mechanisms across nature and society. A hallmark of complex systems is their tendency to exhibit scale invariance and criticality. At critical points, the system becomes poised between competing phases, displaying fluctuations at all scales and giving rise to universal laws that transcend the details of the underlying interactions. Scaling invariance implies that the same structural or dynamical properties repeat across different length and time scales, a property that connects critical phenomena to fractal and multifractal patterns [4–12].

In particular, multifractality reflects the coexistence of multiple scaling exponents, capturing the heterogeneous and hierarchical organization typical of critical dynamics [13]. Therefore, complex systems, criticality, and multifractality are deeply interconnected concepts. Complexity often emerges through collective critical behavior; critical phenomena manifest as scale-invariant structures; and multifractal analysis provides the mathematical framework to characterize the intricate fluctuations observed in these regimes. Understanding the links among these three aspects is essential to unveil the mechanisms that govern the dynamics of natural and social systems, and to identify the universal signatures that appear when systems operate at or near criticality. In the many-body localized regime, eigenstates exhibit a basis-dependent multifractal behavior: they are delocalized but non-ergodic, and the many-body localized transition is marked by a non-universal jump in the multifractal dimensions [14].

https://doi.org/10.1016/j.chaos.2025.117517

Received 28 August 2025; Received in revised form 9 October 2025; Accepted 28 October 2025

^a Departamento de Física, Universidade Federal Rural de Pernambuco - UFRPE, Recife, PE, Brazil

^b Instituto de Física, Universidade Federal de Alagoas - UFAL, Maceió, AL, Brazil

^{*} Corresponding author at: Instituto de Física, Universidade Federal de Alagoas - UFAL, Maceió, AL, Brazil.

^{**} Corresponding authors at: Departamento de Física, Universidade Federal Rural de Pernambuco - UFRPE, Recife, PE, Brazil.

E-mail addresses: fidelis@fis.ufal.br (F.A.B.F. de Moura), anderson.barbosa@ufrpe.br (A.L.R. Barbosa), adauto.souza@ufrpe.br (A.J.F. de Souza).

For example, multifractality has been observed in the magnetization time series of the two-dimensional Ising model near the critical point, identified through generalized Hurst exponents and the singularity spectrum [15]. The sources of multifractality in these time series come from long-term correlations and broad probability density functions. Multifractality also appeared in mesoscopic conductors' magnetic field-induced conductance fluctuations, especially in the quantum conduction regime [16–18]. In the latter case, the externally applied magnetic field induces statistical correlations in the conductance time series. Similarly, mesoscopic fluctuations in the quantum Hall transition are multifractal stochastic phenomena with multiscale hierarchy [19–21]. These studies suggest that multifractality can appear in time series related to magnetic systems, especially near critical points or the quantum regime, and is associated with long-range temporal correlations.

Unlike conventional phase transitions based on symmetry breaking, topological ones are not associated with long-range order. They involve changes in the global properties of a system that are robust to local perturbations. Multifractality provides a sensitive probe of such transitions, revealing complex temporal correlations and offering insights into the stability of critical phases, as illustrated in systems ranging from Weyl semimetals to superconducting films.

The two-dimensional XY model (2D-XY) is the simplest model presenting a topological phase transition [22,23]. This system depicts an infinite-order Berezinskii-Kosterlitz-Thouless (BKT) transition from bounded vortex-antivortex pairs to a phase with unpaired vortices. Besides, the three-dimensional XY model (3D-XY) exhibits a second-order spontaneous symmetry-breaking phase transition, and its critical properties have been accurately obtained by numerical simulations [24,25] combined with finite-size scaling methods and high-temperature expansions. Thus, studying the multifractality of the time series of the XY model's observables is crucial for understanding the complex dynamics of both conventional and topological phase transitions.

In Ref. [26], the renormalization-group approach was introduced to study nonequilibrium phase transitions in infinite lattice systems. Focusing on spinless interacting fermions driven by a longitudinal electric field, the study shows a nonmonotonic phase boundary: weak fields destroy charge order, while strong fields restore it via many-body Wannier-Stark localization. The system exhibits a BKT transition in equilibrium, and in nonequilibrium steady states, currents can flow in the opposite direction to the applied field, resembling an effective negative-temperature distribution.

In the present study, we extensively investigate the multifractal features of time series of magnetization and helicity moduli for the 2D-XY and 3D-XY models. Using multifractal analysis [27], we extract generalized Hurst exponents and singularity spectra, allowing us to quantify the degree of multifractality across temperatures. Our results show that multifractality is maximized near the critical points, with broader singularity spectra in the two-dimensional system, consistent with the BKT transition. In contrast, in three dimensions, the multifractal signatures are sharper and more localized, reflecting the second-order nature of the transition. These findings confirm multifractality as a robust tool to characterize both conventional and topological phase transitions.

2. The XY model, simulation, and multifractal analysis

2.1. Model and simulation

The standard XY model consists of a set of interacting planar rotators, where each rotator's orientation is parametrized by an angle $\theta_i \in [-\pi, \pi]$. Here, we consider rotators occupying the sites of fully periodic square or cubic lattices with a lateral size of L. The system Hamiltonian is given by

$$H = -J \sum_{\langle i,j \rangle} \vec{S}_i \cdot \vec{S}_j = -J \sum_{\langle i,j \rangle} \cos(\theta_i - \theta_j), \tag{1}$$

where $\langle i,j \rangle$ denotes pairs of neighboring sites. We take J=1 without loss of generality. In this work, we focus on 2D-XY and 3D-XY models, obtained through Monte Carlo simulations [28,29]. The three-dimensional case exhibits a conventional second-order continuous phase transition associated with spontaneous symmetry breaking. In contrast, the two-dimensional system undergoes an infinite-order BKT transition [26] driven by the unbinding of vortex–antivortex pairs. The simulations were performed using the standard Metropolis algorithm [30], starting from disordered initial states and evolving the system through successive spin updates. To generate a new configuration, a spin is randomly selected, and a trial rotation is proposed. The new state is accepted with probability

$$P = \min \left[1, \exp(-\beta \Delta E) \right], \tag{2}$$

where β is the inverse temperature and ΔE is the energy difference between the proposed and current states. Time is measured in Monte Carlo time steps, where each time step corresponds to one attempt to update every spin in the system. Concretely, in each time step, we attempt to reflect each spin with respect to a randomly chosen direction \hat{r} in the xy plane [31], i.e.,

$$\vec{S}_i \rightarrow \vec{S}_i - (\vec{S}_i \cdot \hat{r})\hat{r},$$
 (3)

with probability given by Eq. (2).

In two- and three-dimensional systems, simulations start from fully disordered configurations. Observables such as squared magnetization and the helicity modulus are measured at each time step as

$$M^{2}(t) = \frac{1}{N^{2}} \left[\sum_{i} \cos \theta_{i}(t) \right]^{2} + \frac{1}{N^{2}} \left[\sum_{i} \sin \theta_{i}(t) \right]^{2}, \tag{4}$$

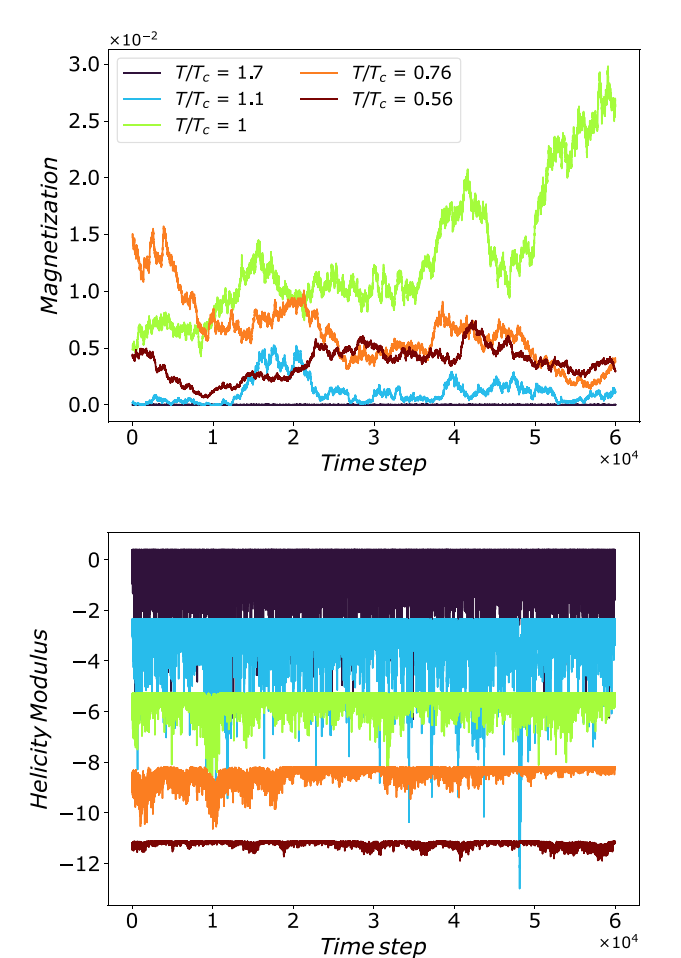


Fig. 1. The typical magnetization (top panel) and helicity (bottom panel) time series for the 2D-XY model and different relative temperature, T/T_c .

$$Y(t) = \frac{1}{N} \sum_{\langle i,j \rangle_{Y}} \cos(\theta_{i} - \theta_{j}) - \frac{\beta J}{N} \left[\sum_{\langle i,j \rangle_{Y}} \sin(\theta_{i} - \theta_{j}) \right]^{2}.$$
 (5)

The sum in (Eq. (5)) is over all links in one direction. The time series of M^2 and Y were generated with 5×10^4 time steps after a warm-up period for several temperatures. Empirically, we found that approximately 2×10^4 time steps is sufficient to avoid bias due to the initial configuration. For each temperature, an ensemble of 20 independent simulations was run. For two-dimensional systems, the lateral size is L = 1024, while for three-dimensional systems, it is L = 64. Fig. 1 shows a typical time series of magnetization and helicity for two-dimensional lattices and different temperatures. In the following, we employ multifractal analysis to characterize the properties of these time series.

2.2. Multifractal analysis

We briefly introduce the Multifractal Detrended Fluctuation Analysis (MF-DFA) [27], applied to the time series of physical observables. For concreteness, we focus on the magnetization time series; however, the same methodology is valid for the helicity time series

Let M_t denote the magnetization in the tth MCS, $t = 1, 2, ..., \eta$, where η is the total number of time steps. We first define the profile of $\{M_t\}$ as follows.

$$\tilde{M}(i) = \sum_{t=1}^{i} (M_t - \langle M \rangle),\tag{6}$$

where

$$\langle M \rangle = \frac{1}{\eta} \sum_{t=1}^{\eta} M_t \tag{7}$$

is the average magnetization time series. The profile $\{\tilde{M}(i)\}$ is divided into $N_s = \operatorname{int}(\eta/s)$ non-overlapping segments of size s, denoted $\{\tilde{M}_j(i)\}$, $j=1,\ldots,N_s$. In each segment, the local trend is removed by fitting a linear function $f_j(i)$, and the variance is calculated as

$$F_s^2(j) = \frac{1}{s} \sum_{i=1}^s \left\{ \tilde{M}[(j-1)s+i] - f_j(i) \right\}^2.$$
 (8)

Next, the qth order fluctuation function is defined as

$$F_q(s) = \left(\frac{1}{2N_s} \sum_{j=1}^{2N_s} \left[F_s^2(j)\right]^{q/2}\right)^{1/q},\tag{9}$$

where q takes several real values: ± 0.2 , ± 0.4 , ± 0.6 , ± 0.8 , ± 1.0 , ± 2.0 , ± 3.0 , ± 4.0 , and ± 5.0 . The sum in Eq. (9) is done from both the beginning and the end of the time series which leads to $2N_s$ segments in total [15]. The scaling behavior of $F_q(s)$ with segment size s is characterized by the generalized Hurst exponent h(q):

$$F_n(s) \sim s^{h(q)}. \tag{10}$$

If h(q) depends on q, the series is multifractal, while if h(q) is independent of q, it is monofractal. The multifractal spectrum is obtained via

$$\tau(q) = qh(q) - 1,\tag{11}$$

and the singularity spectrum $f(\alpha)$ is defined through a Legendre transform:

$$f(\alpha) = q\alpha - \tau(q), \quad \alpha = \frac{d\tau}{da}.$$
 (12)

Multifractal series are characterized by a broad spectrum $f(\alpha)$, while monofractal series produce a narrow spectrum. The strength of multifractality can be quantified by the width $\Delta\alpha = \alpha_{\max} - \alpha_{\min}$; As $\Delta\alpha \to 0$, the series approaches monofractal behavior.

3. Results

This section presents our numerical results for the multifractal analyses of the 2D-XY and 3D-XY models, as discussed above. After an initial warm-up period to eliminate the influence of the starting configuration, we generated time series for the main physical observables. These series, designed to capture temporally correlated fluctuations for multifractal analysis, each contained 5×10^4 time steps. We recorded measurements at every step. Statistical averages were then calculated from an ensemble of 20 independent runs. We chose to focus on two key observables: magnetization and the helicity modulus, see Eqs. (4) and (5). In this way, our Monte Carlo dynamics keeps the temporally correlated fluctuations, which are ideally suited for a multifractal investigation. For consistency, we used 30 bins logarithmically spaced in the interval [100, 12500] for scaling windows, a third-order polynomial for detrending, and 30 values of the moment order q evenly distributed in the interval [-5,5]. This methodology enables us to extract the generalized Hurst exponents and singularity spectra, Eqs. (10) and (12), allowing a quantitative comparison of multifractal properties across different types of phase transition.

3.1. Magnetization

Concerning the 2D-XY model, we recall that magnetization is not an appropriate order parameter for the BKT transition because the system never develops a long-range magnetic order, owing to the Mermin–Wagner theorem [32]. The 3D-XY model exhibits long-range order in the low-temperature phase, and the magnetization works as an order parameter in this case. As we shall see shortly, the multifractal analyses of the magnetization time series signal the phase transition for both models.

Fig. 2 displays the generalized Hurst exponent h(q) as a function of q, derived from the magnetization time series for both 2D-XY and 3D-XY models across various values of T/T_c . In both scenarios, when $T < T_c$ and $T > T_c$, h(q) remains relatively constant or shows only slight variations with respect to q, indicating a monofractal behavior in the magnetization time series. In contrast, at $T \approx T_c$, h(q) exhibits significant variation as a function of q, suggesting a multifractal behavior of the magnetization time series. This observation is further supported by the singularity spectra $f(\alpha)$, which display a narrow width $\Delta \alpha$ for both $T < T_c$ and $T > T_c$, which confirms monofractal behavior. In contrast, when $T \approx T_c$, the width $\Delta \alpha$ becomes noticeably larger, affirming that the magnetization fluctuations are multifractal during the transition.

To highlight the temperature dependence of the multifractal behavior, we analyze the generalized Hurst exponent h(q) as a function of T/T_c for various values of q.

As illustrated in the left and middle panels of Fig. 3, multifractality becomes more pronounced near the critical temperature for both the 2D-XY and 3D-XY models. Notably, the two-dimensional case demonstrates a smoother dependence, which aligns with the infinite-order nature of the BKT transition. In addition, the generalized Hurst exponent exhibits a peak at $1.16T/T_c$, which lies

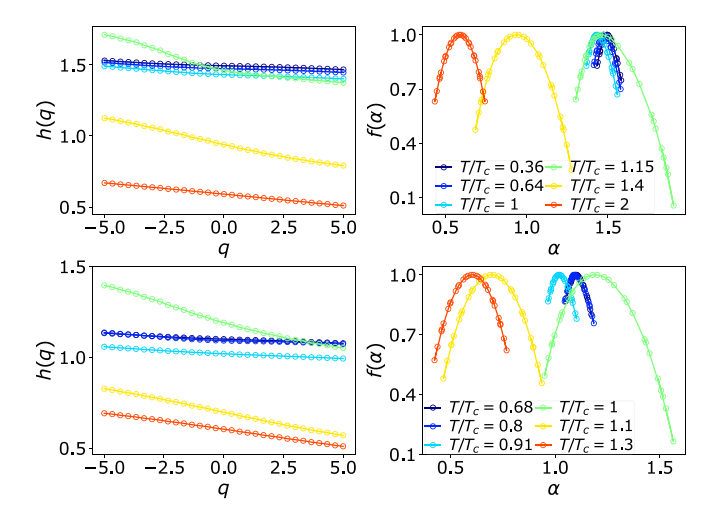


Fig. 2. Ensemble averages of the generalized Hurst exponent h(q) as a function of q (left panel) and the singularity spectrum $f(\alpha)$ as a function of α (right panel) calculated from the magnetization time series of the 2D-XY (top panels) and 3D-XY (bottom panels) models for different values of T/T_c .

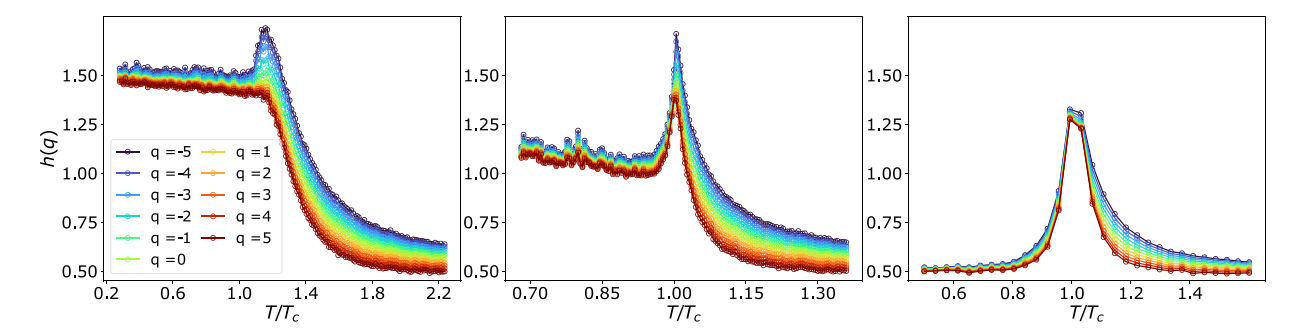


Fig. 3. Ensemble averages of the generalized Hurst exponents h(q) as a function of T/T_c for various values of q calculated from the magnetization time series. The left and middle panels correspond to the 2D-XY and 3D-XY models, respectively. The right panel corresponds to the two-dimensional Ising model, first reported by [15], with a lateral side of L = 1024.

above the nominal BKT transition temperature. Our result is corroborated by high-precision numerical studies of the finite-sized 2D XY model [33], which similarly demonstrate that finite-size effects lead to an observable massless-to-massive crossover at a shifted temperature, specifically near $T/T_c = 1.2$. In contrast, the three-dimensional case shows sharper variations in h(q) near T_c , as expected for a second-order transition. It is striking that the multifractality of the magnetization time series captures the transition temperature for the two-dimensional XY model; see, nevertheless, [34,35].

For a direct comparison, we also include numerical simulations of the two-dimensional Ising model with a lateral size of L=1024, as shown in the right panel of Fig. 3, which were previously reported by [15]. This model exhibits a similar behavior to the 3D-XY model with sharper variations in h(q) near T_c but with distinct scaling properties, thereby highlighting the influence of the universality class on the complexity of the time series.

Fig. 3 also shows a remarkable feature of the generalized Hurst exponent that distinguishes the XY models from the twodimensional Ising model. In the Ising model, the Hurst exponent h(q) approaches 1/2 when the temperature T is below or above the critical temperature T_c . This value, h(q) = 1/2, is characteristic of a monofractal and uncorrelated time series, such as a random walk time series of a Brownian particle. Similar behavior is observed in both the 2D-XY and 3D-XY models when $T > T_c$, implying that all correlations are broken above the critical temperature. For temperatures below the critical temperature $T < T_c$, the Hurst exponent remains approximately constant at a value noticeably above 1/2. Specifically, h(q) is around 1.5 for the 2D-XY model and roughly 1.0 for the 3D-XY model. The higher value of the Hurst exponent in 2D-XY systems can be attributed to the long-range correlations introduced by vortex-antivortex pairs, which form at temperatures below the critical temperature. In contrast, in 3D-XY systems, long-range correlations are weak, leading to a decrease in the value of the Hurst exponent.

Fig. 4 provides a global view of the heat maps of h(q) as a function of T/T_c and q. These diagrams illustrate how multifractality evolves with temperature and moment order, complementing the individual curves presented earlier. The darker and lighter regions on the maps highlight the enhancement of multifractality near criticality, with a strong contrast observed around T_c . This indicates that correlations become more complex and heterogeneous in this regime. The broader variation seen in the two-dimensional

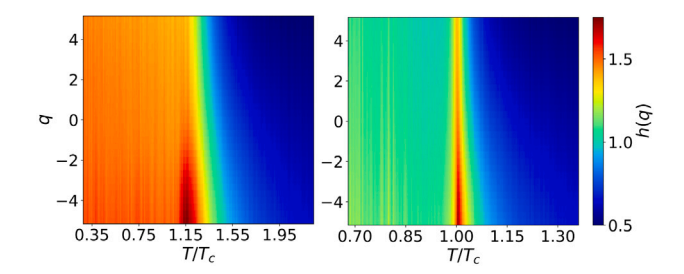


Fig. 4. Heat maps of h(q) as a function of T/T_c and q obtained from the magnetization time series. The left and right panels correspond to the 2D-XY and 3D-XY models.

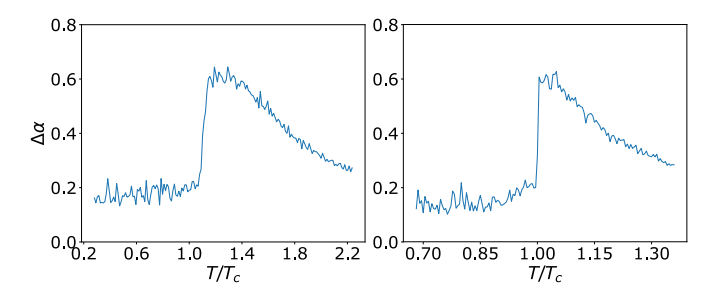


Fig. 5. Singularity spectrum width $\Delta \alpha$ of the magnetization as a function of T/T_c for the 2D-XY (left panel) and 3D-XY (right panel) models.

case suggests stronger multifractality compared to the three-dimensional scenario. This observation is consistent with the longrange correlations generated by the unbinding of vortex-antivortex pairs during the BKT transition. In contrast, the multifractal enhancement in the three-dimensional case is more localized around T_c , reflecting the sharper nature of a conventional second-order phase transition. Thus, the heat maps not only support the quantitative analysis of h(q) but also provide a clear visual representation of the differences between topological and symmetry-breaking critical behaviors.

Finally, Fig. 5 shows the width $\Delta\alpha$ of the singularity spectrum, which serves as a quantitative measure of the strength of multifractality. In both two and three dimensions, $\Delta\alpha$ exhibits a pronounced peak close to T_c , indicating that the temporal fluctuations of the system become maximally complex in the vicinity of the phase transition. The broader peak observed in the two-dimensional case is consistent with the BKT mechanism, where the unbinding of vortex-antivortex pairs gives rise to scale-free correlations across a wide range of temporal and spatial scales. In contrast, the three-dimensional case exhibits a narrower and sharper maximum, reflecting the more localized critical region characteristic of a conventional second-order transition. Therefore, the behavior of $\Delta\alpha$ not only quantifies the strength of multifractality but also provides a clear distinction between the two types of phase transitions, highlighting its usefulness as a diagnostic indicator of criticality.

3.2. Helicity modulus

We now turn our attention to the helicity modulus, which characterizes the phase stiffness of the system and provides direct insight into the rigidity of the spin configuration against twists in boundary conditions. The helicity modulus is a more suitable observable to detect a BKT transition, for it undergoes a universal jump at the transition temperature.

Fig. 6 presents h(q) and $f(\alpha)$ for the helicity time series. For the 2D-XY model, both below and above the critical temperature T_c , the helicity modulus h(q) remains relatively constant or shows only slight variations with respect to q. This behavior indicates a monofractal nature of the helicity time series. However, at $T \approx T_c$, h(q) exhibits significant variation as a function of q, which supports a multifractal behavior of the helicity time series, similar to that of the magnetization behavior, as shown in Fig. 2. In contrast, for the 3D-XY model, h(q) remains relatively constant across the entire temperature range, indicating a monofractal behavior for the helicity time series, differing from the behavior observed in magnetization, Fig. 2. The unusual behavior of the helicity time series can be explained by the fact that in two dimensions, the helicity modulus plays a crucial role in signaling the BKT transition. The singularity spectrum in two dimensions is significantly broader than in three dimensions, reflecting the extended range of correlations that arise from the unbinding of vortex-antivortex pairs. Conversely, the three-dimensional case presents a more compact spectrum, consistent with the sharper nature of a second-order transition. This comparison highlights the complementary role of the helicity modulus analysis in distinguishing between topological and conventional critical behaviors.

We illustrate the temperature dependence of h(q) in Fig. 7. For the 2D-XY model, h(q) increases as the temperature decreases below the transition temperature. In contrast, for temperatures above T_c , $h(q) \rightarrow 1/2$. The 3D-XY model, however, $h(q) \approx 1/2$ whether the temperature is above or below T_c . This difference highlights the fundamentally distinct critical properties of the two transitions. In two dimensions, the BKT transition does not exhibit conventional symmetry breaking, and the system remains critical

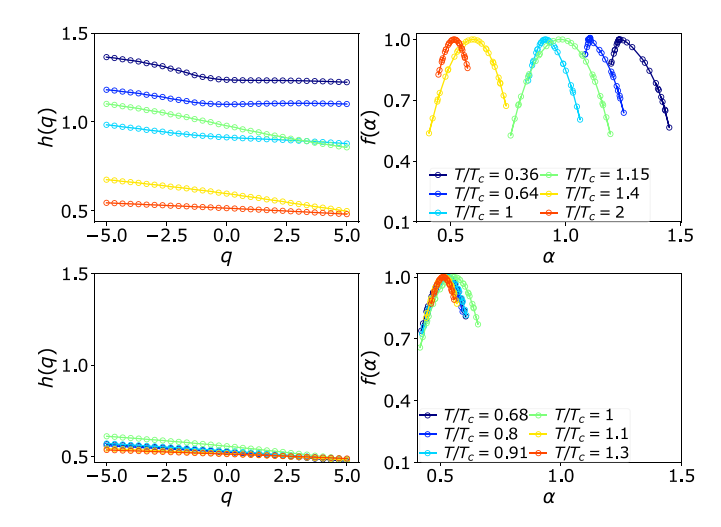


Fig. 6. Ensemble averages of the generalized Hurst exponent h(q) as a function of q (left panel) and the singularity spectrum $f(\alpha)$ as a function of α (right panel) calculated from the helicity moduli time series of the 2D-XY (top panels) and 3D-XY (bottom panels) models for different values of T/T_c .

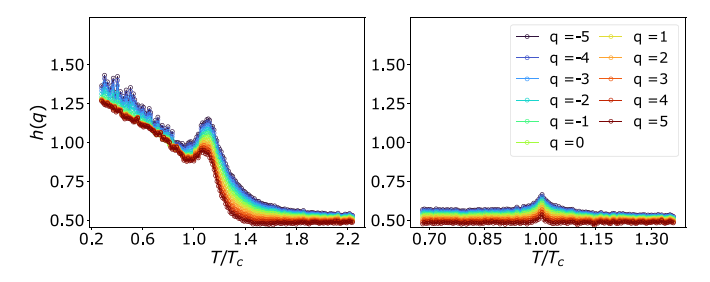


Fig. 7. Ensemble averages of the generalized Hurst exponents h(q) as a function of T/T_c for various values of q calculated from the helicity time series. The left and right panels correspond to the 2D-XY and 3D-XY models, respectively.

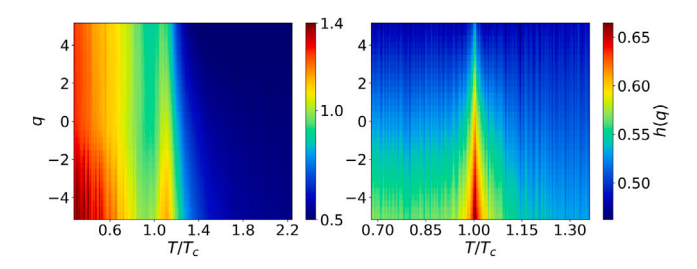


Fig. 8. Heat maps of h(q) as a function of T/T_c and q obtained from the helicity time series. The left and right panels correspond to the 2D-XY and 3D-XY models.

all the way down to zero temperature. In contrast, in three dimensions, the transition displays typical characteristics of a continuous second-order phase transition. The corresponding heat maps in Fig. 8 further validate these observations, demonstrating a critical enhancement of multifractality near and below T_c in two dimensions. Finally, Fig. 9 presents the width of the singularity spectrum, $\Delta \alpha$, as a function of T/T_c . Similarly to the behavior of magnetization, $\Delta \alpha$ peaks near the critical temperature in both the 2D-XY and 3D-XY models, with the BKT transition exhibiting a broader spectrum. Together, these results consistently demonstrate how dimensionality affects both the intensity and spatial distribution of critical fluctuations, highlighting the multifractal nature of the system near T_c across different dimensions.

4. Discussion and conclusions

In this study, we investigated the multifractal properties of time series generated from Monte Carlo simulations of the 2D-XY and 3D-XY models. By applying multifractal detrended fluctuation analysis (MF-DFA) to the time series of magnetization and

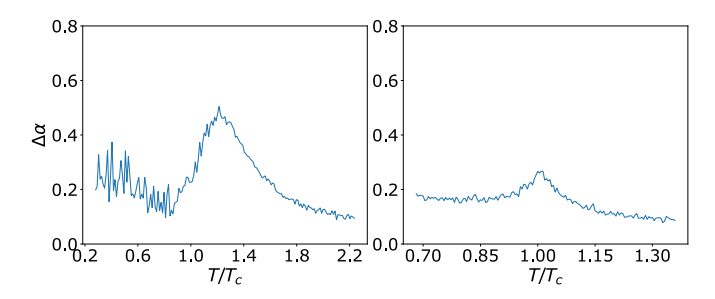


Fig. 9. Singularity spectrum width $\Delta \alpha$ of the helicity as a function of T/T_c for the 2D-XY (left panel) and 3D-XY (right panel) models.

helicity modulus, we characterized the scaling behavior of temporal fluctuations in the critical regions of these systems. Our results demonstrate that multifractality emerges as a fundamental feature of both conventional and topological phase transitions at criticality, whereas monofractality dominates away from the transition. This highlights the potential of multifractal analysis as a complementary approach to more traditional probes of critical phenomena.

From the magnetization time series, we observed that the generalized Hurst exponents h(q) show a pronounced dependence on q at the critical temperature, confirming the multifractal character of the fluctuations. In contrast, below and above T_c , h(q) becomes nearly independent of q, signaling the return to monofractal dynamics. The corresponding singularity spectra $f(\alpha)$ are broad in both two and three dimensions at criticality, while far from T_c they collapse to narrow distributions. Notably, the 2D-XY model exhibits a broader spread of scaling exponents, whereas the 3D-XY model shows sharper but narrower spectra.

These observations are reinforced by the temperature dependence of the width of the singularity spectrum $\Delta \alpha$, which consistently peaks at the transition. The broader peak in two dimensions is fully consistent with the Berezinskii–Kosterlitz–Thouless (BKT) mechanism, where the unbinding of vortex–antivortex pairs generates fluctuations spanning multiple scales. In three dimensions, the second-order character of the transition results in a more localized, yet still significant, multifractal signal. A comparison with the two-dimensional Ising model further strengthens the conclusion that multifractality is not exclusive to the XY universality class. Instead, it appears to be a general hallmark of critical dynamics, with variations reflecting the specific universality class of the transition.

The analysis of the time series of the helicity modulus provided complementary insights. In the 2D-XY model, the helicity modulus quantifies phase stiffness and serves as the order parameter for the BKT transition. Its multifractal fluctuations revealed clear signatures of criticality: as with the magnetization, $\Delta \alpha$ reached a maximum around T_c . Once again, the two-dimensional case was characterized by a broader and smoother spectrum, while the three-dimensional case displayed a narrower but sharper one. The consistency across different observables emphasizes the robustness of multifractality as a diagnostic tool for detecting and characterizing critical behavior.

Taken together, these findings suggest that multifractality captures essential features of both conventional and topological phase transitions. In particular, the observation that $\Delta \alpha$ systematically peaks near criticality indicates that the degree of multifractality can serve as a universal marker of phase transitions, complementing more traditional quantities such as the correlation length, susceptibility, and order parameter fluctuations. This aspect is particularly relevant for the BKT transition, which is notoriously difficult to characterize due to its infinite-order nature. Unlike conventional methods that rely on equilibrium scaling, the multifractal approach identifies criticality directly from the scaling of temporal fluctuations, providing a novel perspective on subtle topological phase transitions.

Beyond the XY model, our results connect to broader developments in statistical and condensed matter physics. Multifractal fluctuations have been observed in a wide range of contexts, including mesoscopic conductance [16], quantum Hall systems [19,20], and the Ising model [15]. This suggests that multifractality is a unifying theme across diverse physical systems, from classical to quantum, and from ordered to disordered media. Our study contributes to this broader picture by showing that even classical spin models with well-established critical properties display multifractal features in their dynamical observables. This supports the view that multifractality is not a secondary byproduct, but rather an intrinsic manifestation of critical dynamics, closely tied to the long-range correlations and broad distributions that define these regimes.

In conclusion, we have shown that multifractal analysis provides a robust and versatile framework for probing both conventional and topological phase transitions. By analyzing the time series of magnetization and helicity modulus in the XY model, we found unambiguous evidence of multifractality, which is maximized at the critical temperature. The contrast between the broader multifractal spectra in two dimensions and the sharper ones in three dimensions reflects the fundamental differences between BKT and second-order transitions. Given its generality, this approach may prove valuable for exploring a wide range of systems, including quantum many-body models, disordered materials, and non-equilibrium critical phenomena. Future research should aim to further investigate the universality of multifractal signatures and to establish whether the degree of multifractality can serve as a predictive indicator of criticality across different universality classes.

CRediT authorship contribution statement

Marcos A.A. de Sousa: Software, Investigation, Formal analysis, Data curation. Francisco A.B.F. de Moura: Writing – review & editing, Writing – original draft, Formal analysis, Conceptualization. Anderson L.R. Barbosa: Writing – review & editing, Writing – original draft, Visualization, Validation, Supervision, Software, Resources, Project administration, Methodology, Investigation, Funding acquisition, Formal analysis, Data curation, Conceptualization. Adauto J.F. de Souza: Writing – review & editing, Writing – original draft, Visualization, Validation, Supervision, Software, Resources, Project administration, Methodology, Investigation, Funding acquisition, Formal analysis, Data curation, Conceptualization.

Declaration of competing interest

The authors declare that they have no known competing financial interests or personal relationships that could have appeared to influence the work reported in this paper.

Acknowledgments

The authors acknowledge the financial and institutional support from CNPq, Brazil, CAPES, Brazil, FAPEAL, Brazil, and FACEPE, Brazil, which made this research possible. We are grateful for their contributions to the development of science and researcher training in Brazil.

Data availability

Data will be made available on request.

References

- [1] Comin CH, Peron TKDM, Silva FN, Amancio DR, Rodrigues FA, Costa LdF. Complex systems: Features, similarity and connectivity. Phys Rep 2020;861:1–?. http://dx.doi.org/10.1016/j.physrep.2020.03.002.
- [2] Romaguera ARC, Vasconcelos JVA, Negreiros-Neto LG, Pessoa NL, da Silva JF, Cadena PG, de Souza AJF, de Oliveira VM, Barbosa ALR. Multifractal fluctuations in zebrafish (Danio rerio) polarization time series. Eur Phys J Phys J E 2024;47(5):29. http://dx.doi.org/10.1140/epje/s10189-024-00423-w.
- [3] Leal FC, Vasconcelos JV, Negreiros-Neto LG, de Oliveira VM, de Souza AJ, Barbosa AL, de C. Romaguera AR. Avalanche dynamics of zebrafish schools: Unveiling self-organization and phase transitions. Phys A 2024;651:130040. http://dx.doi.org/10.1016/j.physa.2024.130040, URL https://www.sciencedirect.com/science/article/pii/S0378437124005491.
- [4] Li Y, Dai C. A multifractal formalism in a probability space. Chaos Solitons Fractals 2006;27(1):57–73. http://dx.doi.org/10.1016/j.chaos.2004.11.088, URL https://www.sciencedirect.com/science/article/pii/S0960077904007659.
- [5] Şahin Telli, Chen H, Zhao X. Detecting multifractality and exposing distributions of local fluctuations: Detrended fluctuation analysis with descriptive statistics pooling. Chaos Solitons Fractals 2022;155:111678. http://dx.doi.org/10.1016/j.chaos.2021.111678, URL https://www.sciencedirect.com/science/article/pii/S0960077921010328.
- [6] Tsvetkov V, Mikheev S, Tsvetkov I, Derbov V, Gusev A, Vinitsky S. Modeling the multifractal dynamics of COVID-19 pandemic. Chaos Solitons Fractals 2022;161:112301. http://dx.doi.org/10.1016/j.chaos.2022.112301, URL https://www.sciencedirect.com/science/article/pii/S0960077922005112.
- [7] Pastén D, Pavez-Orrego C. Multifractal time evolution for intraplate earthquakes recorded in southern Norway during 1980–2021. Chaos Solitons Fractals 2023;167:113000. http://dx.doi.org/10.1016/j.chaos.2022.113000, URL https://www.sciencedirect.com/science/article/pii/S0960077922011791.
- [8] Achour R, Li Z, Selmi B, Wang T. A multifractal formalism for new general fractal measures. Chaos Solitons Fractals 2024;181:114655. http://dx.doi.org/10.1016/j.chaos.2024.114655, URL https://www.sciencedirect.com/science/article/pii/S0960077924002066.
- [9] Ren H, Yu Z-G, Liu J-L. Multifractal analysis of complex networks reconstructed with the geometric information from the embedded hyperbolic space. Chaos: An Interdiscip J Nonlinear Sci 2025;35(5):053144. http://dx.doi.org/10.1063/5.0271980.
- [10] Oliveira F, Lucena I, Ramos J. Multifractal chaos in gravitational waves from binary black hole mergers. Chaos Solitons Fractals 2025;200:116980. http://dx.doi.org/10.1016/j.chaos.2025.116980, URL https://www.sciencedirect.com/science/article/pii/S0960077925009932.
- [11] da Silva ASA, Stosic T, Arsenić I, Menezes RSC, Stosic B. Multifractal analysis of standardized precipitation index in Northeast Brazil. Chaos Solitons Fractals 2023;172:113600. http://dx.doi.org/10.1016/j.chaos.2023.113600, URL https://www.sciencedirect.com/science/article/pii/S0960077923005015.
- [12] Stosic B, Stosic T, Tošić I, Djurdjević V. Multifractal analysis of temperature in Europe: Climate change effect. Chaos Solitons Fractals 2025;196:116386. http://dx.doi.org/10.1016/j.chaos.2025.116386, URL https://www.sciencedirect.com/science/article/pii/S0960077925003996.
- [13] Mandelbrot BB. Intermittent turbulence in self-similar cascades: divergence of high moments and dimension of the carrier. J Fluid Mech 1974;62(2):331–58. http://dx.doi.org/10.1017/S0022112074000711.
- [14] Macé N, Alet F, Laflorencie N. Multifractal scalings across the many-body localization transition. Phys Rev Lett 2019;123(18):180601. http://dx.doi.org/10.1103/PhysRevLett.123.180601.
- [15] Zhao L, Li W, pin Yang C, Han J, Su Z, Zou Y. Multifractality and network analysis of phase transition. PLoS ONE 2016;12. http://dx.doi.org/10.1371/
- [16] Pessoa NL, Barbosa ALR, Vasconcelos GL, Macedo AMS. Multifractal magnetoconductance fluctuations in mesoscopic systems. Phys Rev E 2021;104:054129. http://dx.doi.org/10.1103/PhysRevE.104.054129. URL https://link.aps.org/doi/10.1103/PhysRevE.104.054129.
- [17] Olshanetsky EB, Gusev GM, Levin AD, Kvon ZD, Mikhailov NN. Multifractal conductance fluctuations of helical edge states. Phys Rev Lett 2023;131:076301. http://dx.doi.org/10.1103/PhysRevLett.131.076301, URL https://link.aps.org/doi/10.1103/PhysRevLett.131.076301.
- [18] Pessoa NL, Kwon D, Song J, Bae M-H, Macêdo AMS, Barbosa ALR. Multifractal thermovoltage fluctuations in topological insulators. Phys Rev B 2025;111:L081405. http://dx.doi.org/10.1103/PhysRevB.111.L081405, URL https://link.aps.org/doi/10.1103/PhysRevB.111.L081405.
- [19] Barbosa ALR, de Lima THV, González IRR, Pessoa NL, Macêdo AMS, Vasconcelos GL. Turbulence hierarchy and multifractality in the integer quantum hall transition. Phys Rev Lett 2022;128:236803. http://dx.doi.org/10.1103/PhysRevLett.128.236803, URL https://link.aps.org/doi/10.1103/PhysRevLett. 128.236803.

- [20] Amin KR, Nagarajan R, Pandit R, Bid A. Multifractal conductance fluctuations in high-mobility graphene in the integer quantum hall regime. Phys Rev Lett 2021;129 18:186802. http://dx.doi.org/10.1103/physrevlett.129.186802.
- [21] Pessoa NL, Macêdo AMS, Barbosa ALR. Coexistent multifractal mesoscopic fluctuations in integer quantum Hall and orbital Hall transitions. Phys Rev B 2025;112:L081404. http://dx.doi.org/10.1103/2w4y-jydz, URL https://link.aps.org/doi/10.1103/2w4y-jydz.
- [22] Kosterlitz JM, Thouless DJ. Ordering, metastability and phase transitions in two-dimensional systems. J Phys C: Solid State Phys 1973;6(7):1181. http://dx.doi.org/10.1088/0022-3719/6/7/010, URL http://dx.doi.org/10.1088/0022-3719/6/7/010.
- [23] Kosterlitz JM. The critical properties of the two-dimensional xy model. J Phys C: Solid State Phys 1974;7(6):1046. http://dx.doi.org/10.1088/0022-3719/7/6/005, URL http://dx.doi.org/10.1088/0022-3719/7/6/005.
- [24] de Souza LC, de Souza AJF, Lyra ML. Hamiltonian short-time critical dynamics of the three-dimensional XY model. Phys Rev E 2019;99:052104. http://dx.doi.org/10.1103/PhysRevE.99.052104, URL https://link.aps.org/doi/10.1103/PhysRevE.99.052104.
- [25] Campostrini M, Hasenbusch M, Pelissetto A, Rossi P, Vicari E. Critical behavior of the three-dimensional XY universality class. Phys Rev B 2001;63:214503. http://dx.doi.org/10.1103/PhysRevB.63.214503, URL https://link.aps.org/doi/10.1103/PhysRevB.63.214503.
- [26] Klöckner C, Karrasch C, Kennes DM. Nonequilibrium properties of Berezinskii-Kosterlitz-Thouless phase transitions. Phys Rev Lett 2020;125:147601. http://dx.doi.org/10.1103/PhysRevLett.125.147601, URL https://link.aps.org/doi/10.1103/PhysRevLett.125.147601.
- [27] Kantelhardt JW, Zschiegner SA, Koscielny-Bunde E, Havlin S, Bunde A, Stanley H. Multifractal detrended fluctuation analysis of nonstationary time series. Phys A 2002;316(1):87–114. http://dx.doi.org/10.1016/S0378-4371(02)01383-3.
- [28] Xu W, Sun Y, Lv J-P, Deng Y. High-precision Monte Carlo study of several models in the three-dimensional U(1) universality class. Phys Rev B 2019;100:064525. http://dx.doi.org/10.1103/PhysRevB.100.064525, URL https://link.aps.org/doi/10.1103/PhysRevB.100.064525.
- [29] Landau D, Binder K. A guide to Monte Carlo simulations in statistical physics. Cambridge University Press; 2021, p. i-ii.
- [30] Metropolis N, Rosenbluth AW, Rosenbluth MN, Teller AH, Teller E. Equation of state calculations by fast computing machines. J Chem Phys 1953;21(6):1087–92. http://dx.doi.org/10.1063/1.1699114, arXiv:https://pubs.aip.org/aip/jcp/article-pdf/21/6/1087/18802390/1087_1_online.pdf.
- [31] Wolff U. Collective Monte Carlo updating for spin systems. Phys Rev Lett 1989;62:361–4. http://dx.doi.org/10.1103/PhysRevLett.62.361, URL https://link.aps.org/doi/10.1103/PhysRevLett.62.361.
- [32] Mermin ND, Wagner H. Absence of ferromagnetism or antiferromagnetism in one- or two-dimensional isotropic heisenberg models. Phys Rev Lett 1966;17:1133–6. http://dx.doi.org/10.1103/PhysRevLett.17.1133, URL https://link.aps.org/doi/10.1103/PhysRevLett.17.1133.
- [33] Chung SG. Essential finite-size effect in the two-dimensional XY model. Phys Rev B 1999;60:11761–4. http://dx.doi.org/10.1103/PhysRevB.60.11761, URL https://link.aps.org/doi/10.1103/PhysRevB.60.11761.
- [34] Faulkner MF. Symmetry breaking at a topological phase transition. Phys Rev B 2024;109:085405. http://dx.doi.org/10.1103/PhysRevB.109.085405, URL https://link.aps.org/doi/10.1103/PhysRevB.109.085405.
- [35] Faulkner MF. Emergent electrostatics in planar XY spin models: the bridge connecting topological order with broken U(1) symmetry. New J Phys 2025;27(6):061201. http://dx.doi.org/10.1088/1367-2630/add7fd, URL http://dx.doi.org/10.1088/1367-2630/add7fd.